Acta Mech. Sin. (2011) 27(6):1098–1104
DOI 10.1007/s10409-011-0535-8

TECHNICAL NOTE

Application of color structured light pattern to measurement of large out-of-plane deformation

Xing Lü · Jun-Hong Zhou · Dong-Dong Liu · Jue Zhang

Received: 7 March 2011 / Revised: 24 April 2011 / Accepted: 13 July 2011

Abstract Measurement of out-of-plane deformation is significant to understanding of the deflection mechanisms of the plate and tube structures. In this study, a new surface contouring technique with color structured light is applied to measure the out-of-plane deformation of structures with one-shot projection. Through color fringe recognizing, decoding and triangulation processing for the captured images corresponding to each deformation state, the feasibility of the method is testified by the measurement of elastic deflections of a flexible square plate, showing good agreement with those from the calibrated displacement driver. The plastic deformation of two alloy aluminum rectangular tubes is measured to show the technique application to surface topographic evaluation of the buckling structures with large displacements.

Keywords Out-of-plane deformation · Surface contouring · Color structured light · Plate deflection · Rectangular tube buckling

1 Introduction

The out-of-plane deformation is mostly the major displacements of bent plates, buckling tubes, and other thin-wall structural members. The measurement of this kind of displacement field is significant to evaluation of the deformation modes and understanding of the deflection mechanisms of the structures. For instance, when a thin-wall tube is subjected to axially quasi-static or impact load, large out-of-plane displacement will appear in the normal direction to the tube surface, which offers various buckling modes of the tubes with progressive axial folding [1,2]. In recent years, these structures have attracted increasingly more attention in the design of transportation systems due to their effective capability to absorb kinetic energy during the performance of plastic buckling, to meet increasing demands for using lighter and low-cost aluminum alloy structures in the systems for energy saving and crushing protection [3–5].

Moiré techniques, especially the shadow moiré and projecting moiré, are conventional methods to measure the out-of-plane displacement field. For the cases of large displacement, such as buckling deformation of the plates or tubes, however, the patterns of shadow moiré are normally blur in the deep caved areas due to the large gap between the deformed surface and the grating [6,7]. This problem can be avoided by using the projecting moiré without the trouble of depth of field (DOF) problem. Recognition and processing of the projected fringes, however, remains difficult for a computer software to automatically identify those black-and-white fringes without any specific optical characteristics among them [8–10]. In recent years, the rapid development of digital techniques promotes the applications of digital projection such as LCD or DLP projectors, which have advantages of convenience for use and low cost. Meanwhile, the structured light projections have been developed to provide new methods for surface profilometry and deformation evaluations [11–15]. Apart from applications to online inspection of product quality [16, 17], recognition of robotic sensing in mechanical engineering [18], chest-wall evaluation for lung function estimations in biomedical engineering [19], structure light projection shows its convenience in phase shifting without moving any hard parts of the projector, and easy change of fringe density to alter measurement sensitivity [20].

In this study, a new technique of structured color light is applied to measure the out-of-plane deformation of structure surfaces. During the tests, only one picture is needed

X. Lü · J.-H. Zhou · D.-D. Liu · J. Zhang (✉)
College of Engineering, Peking University,
100871 Beijing, China
e-mail: zhangjue@pku.edu.cn

to be captured for each deformation state so as to obtain the surface profiles based on an imaging processing algorithm. The color pattern is designed by encoding the stripes with color sequences to ensure the formed fringe different from others in the whole pattern, which avoids fringe confusions by providing each stripe with a unique color composition to be identifiable in the processing of the recorded image. Meanwhile, the advantage of projecting moiré remains in the digital projections so that everywhere covered by the pattern can be recorded without DOF limitations, which is especially useful for large displacement field measurement. To validate the technique applicable to large deformation evaluation, an elastic deflection field of a flexible square plate clamped at four edges was measured to evaluate the experimental results with the calibrated data. Moreover, plastic deformation of two alloy aluminum tubes was measured to show the technique application to surface profile estimation of the buckling structures under compression.

2 Experimental procedure

2.1 Optical system

Figure 1 shows the experimental configuration to record the out-of-plane deformation of an object under load. The measurement is based on the triangulation of the projection system, which consists of a DLP projector (HP XB31) for color pattern illumination and a digital camera (Canon 1000D) for image recording. In this layout, the line connecting the center (O_p of the projector and the center O_c of the camera is parallel to a reference plane or the initial plane of the specimen. When the object surface deforms under external force, the projected light Point A on the reference plane moves to the Point C on the deformed surface, which corresponds to the Point B on the reference plane. The triangle ΔABC is similar to $\Delta O_c O_p C$, where the side AB corresponds to a relevant shift d on the image plane of the recording camera. By measuring the in-plane image shift d with $d = AB/k$ (k is the magnification of the camera), the surface height change or the out-of-place displacement w is obtained by [21]

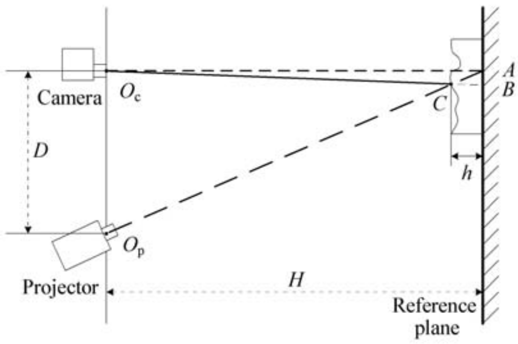

Fig. 1 Optical geometry of pattern projection and imaging for triangulation measurement

$$w = \frac{Hdk}{dk + D}, \tag{1}$$

where H is the distance between the reference plane and the camera, and D is that between the projector and the camera.

2.2 Color structured pattern

A color pattern consisting of parallel straight fringes is utilized to project on the specimen surface. The color form of the whole pattern is encoded by a De Bruijn sequence [3], using four colors (red, yellow, blue, green) with an order of three in the sequence arrangement, as shown in Fig. 2. Unlike the previous study of Chen [21], this system uses only 4 adjacent colors with a black strip at the edge to make up a color fringe, which is unique by color symbols in the whole pattern and the black strip makes each fringe edge sharply recognizable from the others. Based on these color fringes covered on the object surface, every point both on the reference plane of the un-deformed surface and on the deformed specimen is easily identified, which provides the in-plane shift d of the fringes on the pattern images recorded before and after specimen loading, to obtain the corresponding out-of-plane displacement components by using the triangulation principle given above.

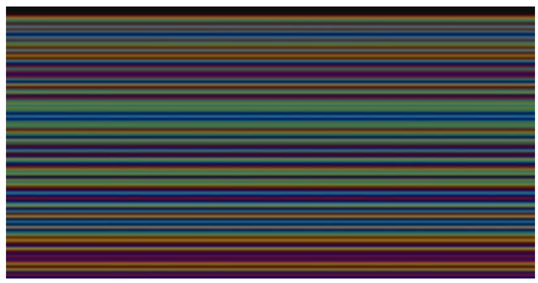

Fig. 2 The projection pattern encoded by 4 color symbols with De Bruijn sequence and a black strip between the adjacent color fringes

2.3 Color image processing

Before and after the loading acts on the specimen, the color structured patterns projected on the object surface are captured by one-shot exposure of the camera for each deformation state. The reference image and the deformed image recorded are then processed to obtain the displacement field.

Post-processing is firstly carried out to segment the color patterns by color space conversion. After apparent errors and perturbations are eliminated through interception, the image is transformed from RGB to HSV color space. In the HSV color space, the value of hue is not affected by the color brightness and saturation. Thus the second derivative of brightness is used to binarize the brightness of the image, given by

$$f'(i) = \sum_{j=1}^{R/2} [f(i+j) - f(i-j)], \tag{2}$$

where f is the original gray distribution of the projection model, i is the element index, and R is the order of the linear derivation filter that should be less than the width of the color stripes [22]. In other words, after calculating the second derivatives for each row of the image, the points with the values greater than 0 are put into the background and the others are classified as the points in the stripes.

For the fringes line by line, the center locations of the stripes are determined in the segmented regions by using a normalized centroid algorithm,

$$M_{\text{center}} = \sum_{i \in E}^{i} I(i)x(i) \Big/ \sum_{i \in E}^{i} I(i), \tag{3}$$

where I is the gray function in the segmentation region, x is the coordinate function, i is the pixel index, and E is the normalized intensity. Meanwhile, the color fringes are identified by their code words. To eliminate the noise effect in recognition, a mean threshold is computed by averaging the hue values of the pixels

$$H_{\text{mean}} = \sum_{i \in E}^{i} I(i) \Big/ \sum_{i \in E}^{i} I. \tag{4}$$

Therefore, the spatial code words of each strip are decoded for the color structured patterns. In this way, the position difference d between the images of the deformed pattern and the reference pattern is easily determined by matching the code words of the fringes, which provides the measured data to calculate the out-of-plane displacement field as the topographic change of the surface height.

3 Results and discussion

3.1 Displacement measurement of bent square plates

To validate the color structured light method, the deflection field of a flexible plastic plate was measured. The four edges of the square plate were fixed in a steel frame and the back center of the plate was loaded by a mechanical driver with calibration scale. The screw driver could produce the minimum calibrated displacement of 0.25 mm and the largest movement distance of 30 mm. Before the force was applied on the plate, the color fringe pattern was projected on the specimen surface to record the reference pattern as the straight strips with uniform pitch. With the deformation of the plate under lateral concentrated load, the distorted color fringes were captured with one-shot recording for each loading step. Figures 4a and 4b show examples of those patterns with displacements of the driver at the plate center to be 4 mm and 8 mm, respectively. By using the image processing mentioned above, the out-of-plane displacement contours are obtained as shown in Figs. 4c and 4d, corresponding to the color fringe patterns with mm as the displacement unit in the maps.

In the image processing of the color structured patterns, a 9×9 (pixel) median filtering was performed to reduce the salt and pepper noise involved due to the non-uniform light reflection of the plate surface. As a comparison, a series of deflection data along the central line of the plate are obtained as shown in Fig. 5a, with the movement of the loading driver from 2 mm to 8 mm step by step with 0.5 mm displacement intervals. Moreover, the peak displacements measured at the

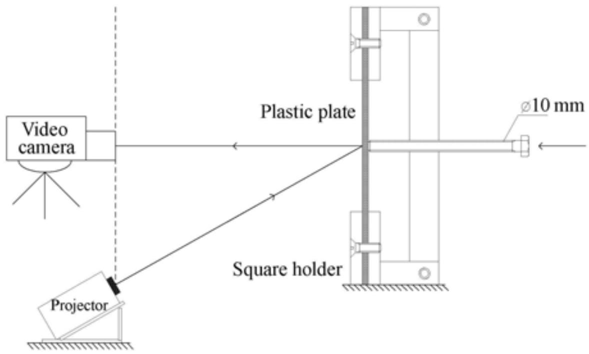

Fig. 3 Set-up for elastic deformation measurement of a bending plate loaded at the center of the plate back

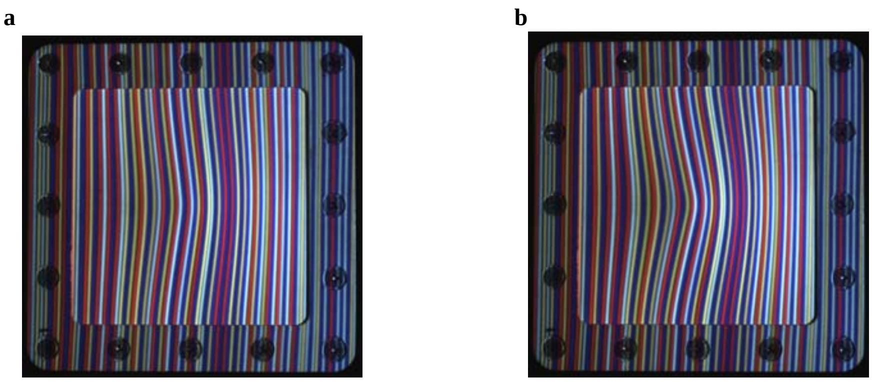

Fig. 4 Projection patterns modulated by elastic deformation of the bent plate as the center displacements are **a** 4 mm; **b** 8 mm; **c** and **d** the corresponding contours of the displacement field

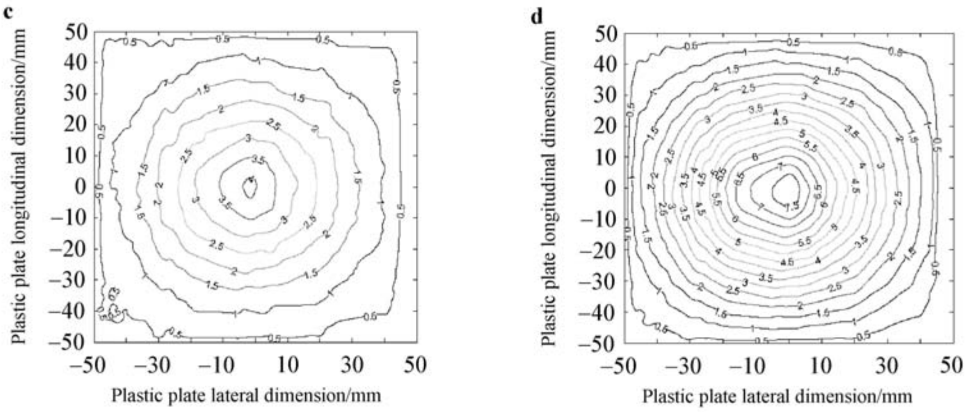

Fig. 4 Projection patterns modulated by elastic deformation of the bent plate as the center displacements are **a** 4 mm; **b** 8 mm; **c** and **d** the corresponding contours of the displacement field (continued)

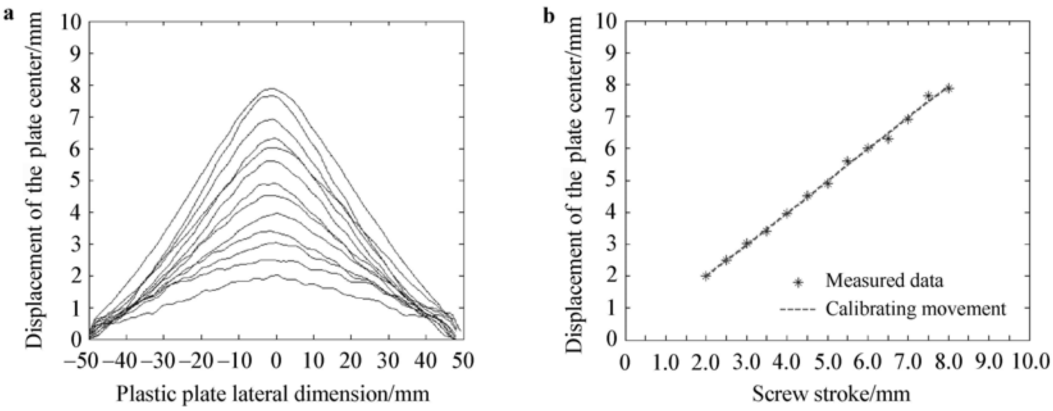

Fig. 5 **a** Displacement profiles along the central line of the plastic plate with the increase of loading displacement from 2 mm to 8 mm; **b** Comparison between peak deflection of the plate and calibrating movement of the driver scale

plate center are compared with the calibrating line from the movement of the load driver, as given in Fig. 5b, showing good agreement in the elastic deformation with a relative mean error less than 2%. Although every step of load changing is under careful operation, errors are still inevitable during manual adjustment of the screw driver and some are due to systemic errors.

3.2 Deformation profiles of buckled tubes

An important application of this work is topographic estimation of the deformed surface of aluminium alloy tubes buckled by compression. With advantages of light weight and reasonable intensity, this kind of structure has satisfactory properties of energy absorption by its performance of plastic deformation and buckling under quasistatic and impact loads. With development of the progressed buckles, the topographies of the thin walls provide various buckling modes for the analyses of the tubes under axial folding. In this work, the largely deformed surfaces of two rectangular tubes are evaluated by the color structured light technique. The initial sizes of those tubes are presented in Table 1, whose main differences rely on their cross sections. Under axial compressions loaded by a test machine, the specimens were progressively folded with plastic buckling of the thin walls.

Table 1 Basic information of the aluminum alloy tubes

(Unit: mm)

Tubes	Length		Width	Height	Wall thickness
	before	after			
Type I	200	175	75	26	1.5
Type II	200	170	75	43	1.5

To compare the present method of color fringe projection with conventional techniques of moiré measurement, we firstly give a black-white fringe pattern from shadow moiré projection on a buckling tube, as shown in Fig. 6, where a grating with a pitch of 1 mm per line is placed in the front of the plastically deformed surface. As the superposition of the grating and its shadow, the fringes of shadow moiré in the concave region with large distances between the grating and the deformed surface present a blur pattern due to DOF problem of imaging, as shown in Fig. 6, dedicated by the dotted boxes.

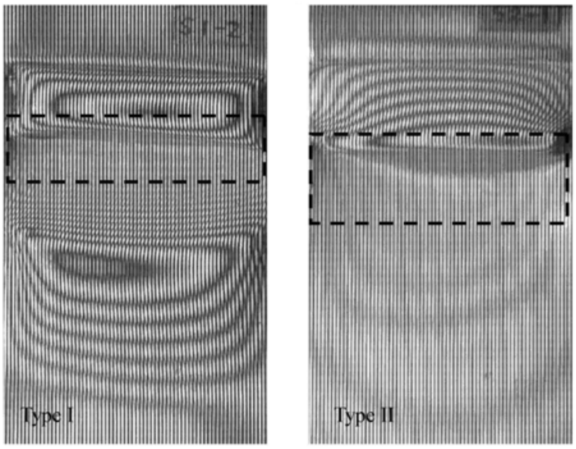

Fig. 6 Black- and -white fringe pattern from shadow moiré projection on the buckling tubes, where the dotted boxes include blur fringes caused by depth of focus problem

This kind of fringes brings much difficulty of pattern recognition to image processing of computers, and produces large errors for displacement measurement. By contrast, the technique of structured color pattern projection avoids this problem—the fringes on the deformed surface are all clearly visualized, as shown in Figs. 7a and 8a, both on the raising parts and in the concave areas of the buckling surface. Moreover, the color-encoded fringes are easily recognized in image processing of computers, as the algorithms mentioned above are utilized, which produce accurate full-contour of the deformed surface.

Figure 7 shows the example result for the Type I tube, where Fig. 7a gives the color fringe pattern projected on the front surface of the deformed tube, Fig. 7b presents the contour map of the bulked surface of the tube in that plastic deformation state, and Fig. 7c is the 3-D plot of the deformation profile. Figure 8 gives similar results for the Type II tube, showing the color strips spatially modified by the bulked surface, and the out-of-plane distribution of the deformed surface. It is apparent that the fringes projected on the folded tube are very clear without any problem of DOF for image focusing, which is a big trouble for shadow moiré method as the large distances between the deeply deformed surface and the grating in the front of the specimen make the fringes undistinguishable. With the help of the image processing presented above, the color fringes are recognized for every point on the illuminated surface, and the topographies of the deformed structure are obtained by solving the distortion of the image fringes with the triangulation computations.

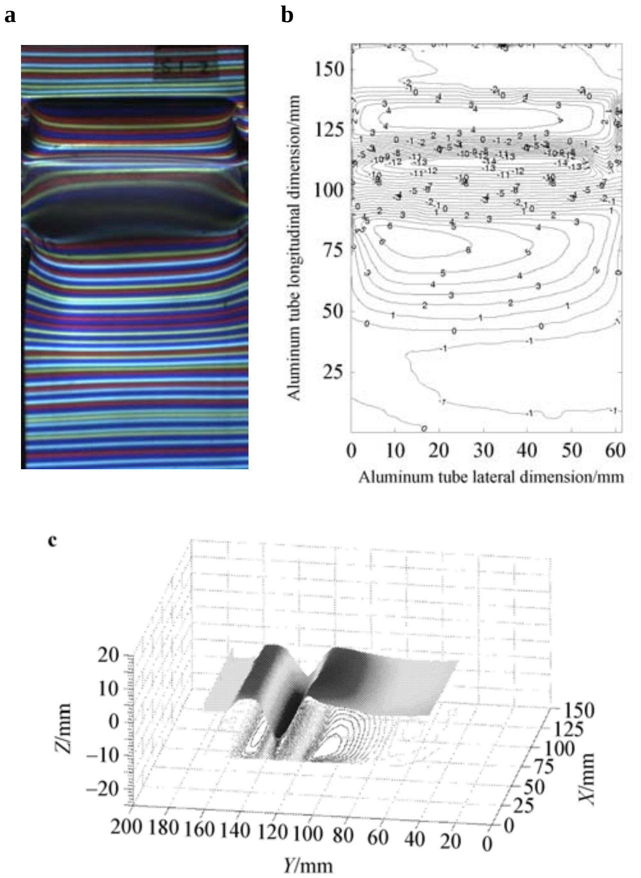

Fig. 7 **a** Color fringe pattern projected onto the buckled surface of Type I rectangular tube; **b** Deformation field represented by the contour map; **c** 3-D topographic plot of the buckling tube

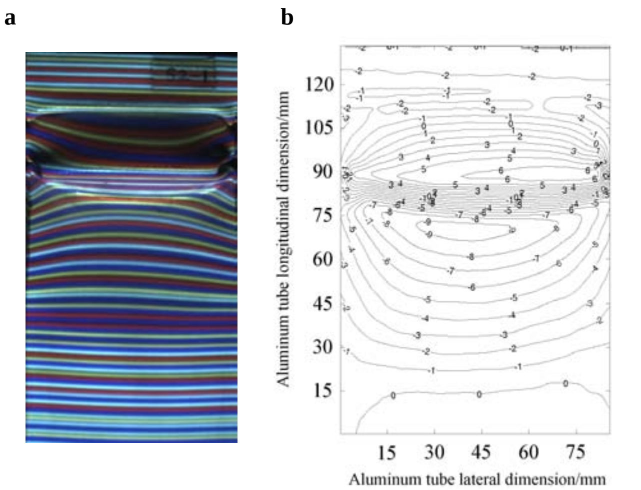

Fig. 8 **a** Color structured fringes projected onto the buckled surface of Type II rectangular tube; **b** Contours of the deformation field; **c** 3-D topographic plot of the buckling surface

c

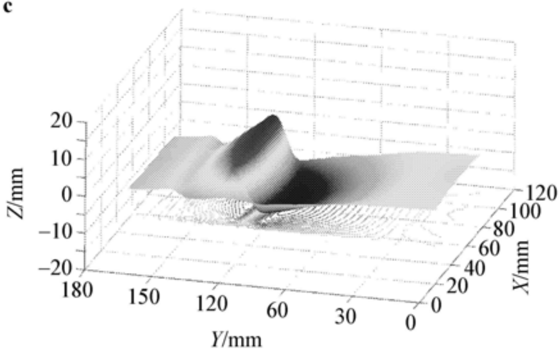

Fig. 8 **a** Color structured fringes projected onto the buckled surface of Type II rectangular tube; **b** Contours of the deformation field; **c** 3-D topographic plot of the buckling surface (continued)

4 Conclusion

This note demonstrates the applications of color structured light method to the out-of-plane deformation measurement of largely deformed structures. The color fringes are designed on the basis of one-shot strategy of projection on the deformation surface, consisting of the stripes encoded by the color symbols with unique sequence in the whole pattern. The black stripes involved in the adjacent color fringes make the sharp-edged fringes recognizable in combination with the color sequences. Using post-processing and triangulation computations for the captured images, the feasibility of the one-shot technique was testified by the measurement of elastic deflection field of a flexible square plate fixed at four edges. The results are in good agreement with those of the calibrated displacement driver. The plastic deformation of two alloy aluminum tubes with rectangular cross-sections was measured to show the technique application to surface topographic evaluation of the buckling structures with large deformation. In fact, the one-shot technique not only provides the method of color light structured projection, simple and convenient ways for the out-of-plane displacement measurement, but also offers strong potentials with video-based recording for the high speed measurement of dynamic structures under impact load. At present, the technique is applicable to measure the out-of-plane displacements of initially flat surfaces. The application to the curvature surfaces, such as on the circular tubes under buckling, needs further studies to avoid the shadows of pattern projection and to develop complicated algorithms for 3-D topographic reconstructions.

References

1 El-Hage, H., Mallick, P.K., Zamani, N., et al.: A numerical study on the quasi-static axial crush characteristics of square aluminum-composite hybrid tubes. Composite Structures **73**(4), 505–514 (2006)
2 Karagiozova, D.: Dynamic buckling of elastic-plastic square tubes under axial impact—I: Stress wave propagation phenomenon. International Journal of Impact Engineering **30**(2), 143–166 (2004)
3 Zhu, L., Yu, T.X.: Saturated impulse for pulse-loaded elastic-plastic square plates. International Journal of Solids and Structures **34**(14), 1709–1718(1997)
4 Huang, X., Lu, G., Yu, T.X.: Collapse of square metal tubes in splitting and curling mode. Journal of Mechanical Engineering Science **220**(1),1–13 (2006)
5 Zhang, X.W., Su, H., Yu, T.X.: Energy absorption of an axially crushed square tube with a buckling initiator. International Journal of Impact Engineering **36**(3), 402–417 (2009)
6 Degrieck, J., Paepegem, W., Boone, P.: Application of digital phase-shift shadow moiré to micro deformation measurements of curved surfaces. Optics and Lasers in Engineering **36**(1), 29–40 (2001)
7 Chen, F., Brown, G., Song, M.: Overview of three-dimensional shape measurement using optical methods. Optical Engineering **39**(1), 10–22 (2000)
8 Choi, Y.B., Kim, S.W.: Phase-shifting grating projection moiré topography. Optical Engineering **37**(3), 1005–1010 (1998)
9 Hai, D., Powell, R.E., Hanna, C.R.: Warpage measurement comparison using shadow moiré and projection moiré methods. Transactions on Components and Packaging Technologies **25**(4), 714–721 (2002)
10 Sciammarella, A.C., Sciammarella M.F.: High-accuracy contouring using projection moiré. Optical Engineering **44**(9), 093605 (2005)
11 Grytten, F., Fagerholt, E., Auestad, T.: Out-of-plane deformation measurements of an aluminium plate during quasi-static perforation using structured light and close-range photogrammetry. International Journal of Solids and Structures. **44**, 5752–5773 (2007)
12 Fechteler, P., Eisert, P.: Adaptive colour classification for structured light systems. Computer Vision, IET **3**(2), 49–59 (2009)
13 Sansoni, G., Carocci, M., Rodella, R.: Calibration and performance evaluation of a 3-D imaging sensor based on the projection of structured light. Transactions on Components and Packaging Technologies **49**(3), 628–636 (2000)
14 Ricardo, L.S., Thorsten, B., Werner, P.J.: Accurate procedure for the calibration of a structured light system. Optical Engineering **43**(2), 464–471 (2004)
15 Chen, S.Y., Li, Y.F. Zhang, J.W.: Vision processing for realtime 3-D data acquisition based on coded structured light. Transactions on Image Processing **17**(2), 167–176 (2008)
16 Song, L.M., Qu, X.H., Yang, Y.G., et al.: Application of structured lighting sensor for online measurement. Optics and Lasers in Engineering **43**(10), 1118–1126 (2005)
17 Brosnan, T., Sun, D.W.: Improving quality inspection of food products by computer vision-a review. Journal of Food Engineering **61**(1), 3–16 (2004)
18 Le Moigne, J.J., Waxman, A.M.: Structured light patterns for robot mobility. Journal of Robotics and Automation **4**(5), 541–548 (1988)
19 Chen, H.J., Cheng, Y., Liu, D.D., et al.: Color structured light system of chest wall motion measurement for respiratory volume evaluation. Journal of Biomedical Optics **15**(2), 026013

(2010)
20 Grytten, F., Fagerholt, E. Auestad, T.: Out-of-plane deforma tion measurements of an aluminium plate during quasi-static perforation using structured light and close-range photogram 409 metry. International Journal of Solids and Structures **44**, 5752–5773 (2007)
21 Chen, H.J., Zhang, J., Fang, J.: Surface height retrieval based on fringe shifting of color-encoded structured light pattern. Optics Letters **33**(6), 1801–1803 (2008)
22 Pages, J., Salvi, J., Collewet, C., et al.: Optimised De Bruijn patterns for one-shot shape acquisition. Image and Vision Computing **23**, 707–720 (2005)